Large Two-Photon Cross Sections and Low-Threshold Multiphoton Lasing of CdS/CdSe/CdS Quantum Shells

Benjamin T. Diroll,[1*] James P. Cassidy,[2] Dulanjan Harankahage,[2] Xiao-Min Lin,[1] Mikhail Zamkov[2]

[1]*Center for Nanoscale Materials, Argonne National Laboratory. 9700 S. Cass Avenue, Lemont, Illinois 60439, United States*

[2]*The Center for Photochemical Sciences and Department of Physics, Bowling Green State University, Bowling Green, Ohio 43403, United States*

KEYWORDS. Quantum shell, optical gain, amplified spontaneous emission, two photon absorption, laser

ABSTRACT.

Colloidal quantum shells are spherical semiconductor quantum wells, ~~materials~~ which have shown strong promise as optical materials, particularly in classes of experiments requiring multiple excitons. The two-photon properties of CdS/CdSe/CdS quantum shell samples are studied here to demonstrate large non-linear absorption cross-sections while retaining advantageous multiexciton

physics conferred by the geometrical structure. The quantum shells have large per particle two-phonon cross sections (up to 10^7 GM), which highlights their potential use in upconversion imaging. On a volumetric basis, two-photon cross sections traverse values of zero-dimensional quantum dots at small radius to two-photon cross sections similar to two-dimensional nanoplates at larger radii. Time-resolved measurements confirmed that the quantum shells have long biexciton lifetime (>10 ns) and large gain bandwidth (>300 meV). The combination of these attributes with large two-photon cross sections makes the CdS/CdSe/CdS quantum shells excellent gain media under two-photon excitation. Due to a broad gain bandwidth, quantum shell solids support multimodal amplified spontaneous emission from excitons, biexcitons, and higher excited states. Thresholds for amplified spontaneous emission and lasing, which are as low as 1 mJ·cm^{-2}, are comparable or lower than the thresholds reported for other colloidal materials.

Colloidal quantum shells (QSs), in which a narrow band gap spherical shell ~~material is sandwiched as a spherical shell~~ is sandwiched ~~coating~~ between a wider band gap core and ~~outer shell~~surface potential barriers, have recently ~~demonstrated~~ shown promise as nanoscopic optical materials.[1–9] They offer a distinct form of quantum confinement based upon the thickness of the shell material, between that of flat quantum wells and quasi-spherical quantum dots.[1,3,10–17] Although there are a number of QS structures, the most sophisticated in terms of synthetic development are CdS/CdSe/CdS concentric nanostructures, in which quantum confinement of the CdSe layer dictates their optical properties.[1,15] The large physical dimensions of QSs, which have been prepared with diameters greater than 15 nm,[1] decouples the physical size of the nano-object from quantum confinement.[10,15] One important result of this dimensionality control is the highly-effective suppression of Auger recombination, resulting in long biexciton lifetimes, more radiative

Commented [MAZ1]: I like this statement but I think it could be moved to the main text, which would keep the abstract nice and concise. Just a suggestion

Commented [DBT2]: 10.1021/acsphotonics.0c00812 – suppressed Auger; low threshold 1 photon; 1ns biexciton/auger

10.1021/acsenergylett.2c00153
10.1039/D1NR04781G – also multiexcitons citation

Commented [MAZ3]: If you'd like, we can add the QDQW references from the recent ZnS-coated QS paper (Refs. 32-38)

Commented [DBT4R3]:

10.1063/1.2119423 - laser

10.1103/PhysRevB.64.245329

Weller early 90s to properties section
10.1021/j100122a026
10.1103/PhysRevB.49.17072
10.1016/0009-2614(93)80076-2

emission from biexcitonic states, long optical gain lifetime, and broad optical gain bandwidths.[8,9,18]

This work leverages these promising elements of quantum shell materials with below band gap excitation to demonstrate their utility in two-photon applications. Non-linear optical properties and two-photon absorption in particular is important for imaging and microscopy resolution, particularly in biology,[19,20] and valuable for optically-pumped laser applications in which frequency upconversion is desired.[21–33] Here, it is found that the CdS/CdSe/CdS QSs have large two-photon cross sections which depend on the radius of curvature of the QS. Large two-photon cross sections of particles (up to 10^7 GM) indicate that such QS are potentially useful agents for imaging and tagging. A combination of advantageous multiexciton properties and large two-photon cross sections of QSs has been utilized to showcase low-threshold multiphoton excited optical gain, amplified spontaneous emission, and lasing. Optical pumping thresholds as low as

1 mJ·cm^{-2} have been achieved.

1 mJ·cm^{-2} have been achieved.

Results and Discussion.

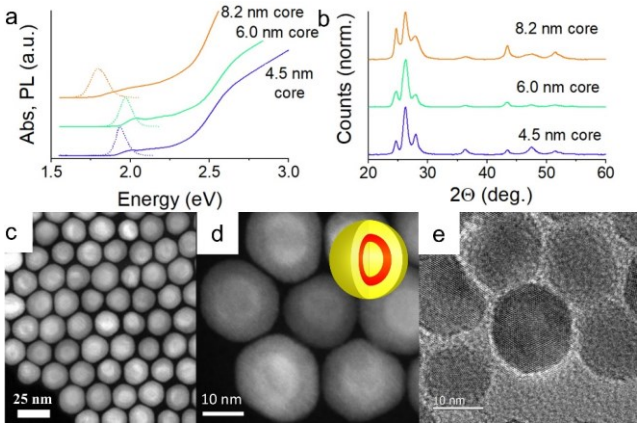

Figure 1. (a) Absorption (solid lines) and photoluminescence (dashed lines) of CdS/CdSe/CdS quantum shell samples. (c) Powder X-ray diffraction of the QSs. (c-d) Dark field transmission electron microscopy images of 8.2-nm-core quantum shell samples. Inset in (e) is a cartoon model showing the structure of the samples, with yellow representing CdS and red CdSe. (e) Bright field TEM image of 6.0-nm-core quantum shell sample.

Figure 1 shows optical and structural characterization of the QS samples used in this work, which are identified by their respective CdS core sizes. The core/shell/shell geometry of the samples was obtained by the triple-stage colloidal growth procedure, similar to earlier works.[2,18] Absorption and photoluminescence spectra are shown in Figure 1a. Due to the large volume of CdS, the absorption above 2.5 eV is much larger than the absorption of the CdSe QS, but photoluminescence under weak excitation derives only from the narrow band gap CdSe. As shown in Figure 1b QSs have a wurtzite crystal structure matching CdS, the dominant constituent of the QSs, and the concentric core/shell/shell geometry is apparent in dark field images in Figures 1c and 1d, with the inset of Figure 1d showing the idealized geometry. Enhanced contrast of the core/shell interface may derive both from composition (Z-contrast) and strain at the interface.[34] The bright field image in Figure 1e shows that the wurtzite crystal lattice is apparent through the entire particle. Additional microscopy images can be found in Figure S1.

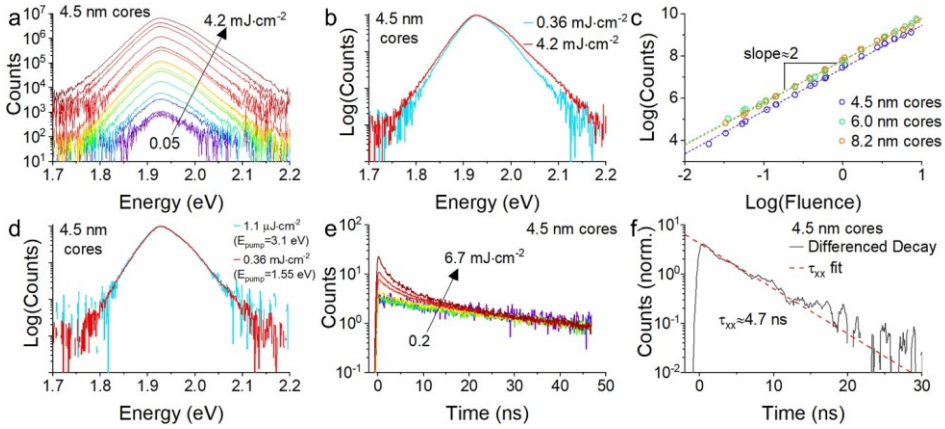

Figure 2. (a) Photoluminescence intensity with increasing pump 1.55 eV pump fluence for sample 4.5 nm core QSs. (b) Normalized spectra of 4.5 nm core QSs at different specified pump fluences. (c) Log-Log plot of integrated photoluminescence counts versus fluence for the three QS samples. Log of fluence is taken for the value in mJ·cm^{-2}. Dashed lines indicate linear slopes of close to 2 for each. (d) Normalized photoluminescence spectrum of 4.5 nm core QSs with specified fluences of 3.10 eV and 1.55 eV excitation. (e) Time-resolved photoluminescence of 4.5 nm core QSs normalized at ~50 ns delay for a series of increasing pump fluence. (f) Differenced data from (e) showing the residual counts from data collected at a fluence of 1.58 mJ·cm^{-2} after subtracting the average counts of 0.24-0.61 mJ·cm^{-2}. A dashed red line indicates a monoexponential fit to estimate the biexciton lifetime under two photon excitation.

Representative fluorescence data ~~of fluorescence~~ from the quantum shell samples under two photon excitation is shown in Figure 2a using the sample with 4.5 nm CdS cores. Figure 2 shows the intensity-dependent spectra for the 4.5 nm CdS core sample and Figure 2b shows a log-log plot of the power-dependent emission for all three samples which confirms the two-photon absorption process with slopes of 1.99±0.02, 2.08±0.02, and 2.01±0.01 for 4.5 nm, 6.0 nm, and 8.2 nm QS cores, respectively. Figure 2c show the spectra normalized at the peak intensity. At low intensity, the spectra of the samples under one- and two-photon excitation are superimposable (Figure 2d). At higher intensities, such as the higher power two-photon excitation shown in Figure 2b, there is an increase in intensity of the blue side of the photoluminescence feature. This feature, which is common to the QSs, is due to emission from doubly-excited biexciton emission. In

particular, the blueshift observed with respect to the exciton emission is, for these CdS/CdSe/CdS QDs, is due to a repulsive biexciton binding energy—slightly higher in energy than excitons. For the QS samples, this biexciton binding energy ($E_{b,xx}$) is estimated using power-dependent spectra to be -48 meV, -64 meV, and -54 meV for the 4.5 nm, 6.0 nm, and 8.2 nm cores, respectively. The repulsive biexciton energies confirm a type-II or quasi-type II band alignment, with substantial delocalization of the electron into CdS, similar to what is observed in certain CdSe/CdS NRs.[35,36] Formation of biexcitonic species is also manifest through the emergence of a faster decay feature in fluence-dependent time-resolved photoluminescence data in Figure 2e. Following Klimov,[37] differencing normalized dynamics above the threshold at which biexcitonic decay is apparent and low-fluence data with two-photon excitation yields an estimate of the biexciton lifetime, here of 4.7 ns. This is very close to the biexciton lifetime extracted under one-photon excitation (see Supporting Information Figures S2 and S3). The biexciton lifetime of the 6.0 nm core and 8.2 nm core samples are 6.7 ns and 11.9 ns, respectively (see Table 1). Biexciton lifetimes in nanosecond time-range are a consequence of the repulsive nature of exciton-exciton interactions and the geometry of the QSs, which suppresses Auger recombination rates, the primary mechanism of biexciton recombination.[37] Biexciton lifetimes are important for determining the threshold of lasing under continuous or electrical injection and QS show among the longest biexciton lifetimes of nanocrystal systems.[38] The biexciton lifetimes of the QS samples are, for example, substantially longer than bare CdSe dots,[39] core/shell structures with sharp interfaces,[40,41] and nanoplatelets[42] (all sub-nanosecond); the ensembles of QSs show longer biexciton lifetimes than the best single particle measurements of graded core/shells with suppressed Auger.[40,43,44]

The two-photon cross sections of the samples was calculated using an approach developed earlier,[45,46] in which standards of known quantum yield and two photon cross section are used

similar to the calculation of comparative quantum yield. According to this methodology, the two-photon cross section of an unknown ($\sigma_x^{(2)}$) depends on the one-photon cross section ($\sigma_x^{(1)}$), fluorescence intensity under one- and two-photon excitation ($F_x^{(n)}$), and quantum yields (η) of the unknown and a reference dye:

$$\sigma_x^{(2)} = \frac{\sigma_{ref}^{(2)}\sigma_x^{(1)}}{\sigma_{ref}^{(1)}} \cdot \frac{F_x^{(2)}}{F_{ref}^{(2)}} \cdot \frac{F_{ref}^{(1)}}{F_x^{(1)}}.$$

This equation is only true if the quantum yield of the sample and the reference dye are assumed to be the same under both one-and two-photon excitation ($\eta^{(2)} = \eta^{(1)}$), an assumption which is substantiated here by identical lifetime (Figure S4) and spectrum of the fluorescence (Figure 2d) under one- and two-excitation.[45] Several parameters can be measured directly or inferred; most parameters of the reference dye, Rhodamine 6G, are taken from literature.[47–49] The cross-section of the samples is ascertained through measurement of the cadmium concentration of digested QSs with known absorption properties and known particle size from TEM, using inductively-coupled plasma optical emission spectroscopy (ICP-OES). Extinction coefficients and one-photon cross-sections calculated using this method for the samples used in this work are given in Table 1. The ratio of $F_x^{(1)}/F_{ref}^{(1)}$ is the ratio of quantum yields under one-photon excitation; the ratio $F_{ref}^{(2)}/F_x^{(2)}$ is calculated from fluence-dependent two-photon photoluminescence. The two-photon cross-sections of the QS samples, in Goeppert-Mayer (GM) units, ranged from 2.22-9.58×10^6 GM. On an absolute scale, such two-photon cross sections are comparable to the very large cross sections reported for cadmium selenide nanoplatelets, which greatly exceed those of QDs or CdSe/CdS nanorods.[45,50] Large per particle two-photon cross sections marks the QSs out as strong candidates for two-photon imaging applications. On a volumetric basis ($\sigma_x^{(2)}/V$), the QSs have two-photon

cross sections which range from comparable to quantum dots (4.9×10^{-27} cm·s for the 4.5 nm cores) to similar to CdSe nanoplatelets (4.9×10^{-26} cm·s for 8.2 nm cores).[45] This suggests that the advantages of the two-dimensional nanoplatelet geometry for two-photon absorption can be partially recaptured in QSs for larger cores sizes with larger radii of curvature, although most two-photon absorption is still occurring in the CdS layers.

Table 1. Properties of Quantum Shell Samples

Size[a] (core)	E_{PL}[b] (eV)	ε[c] (3.1 eV) ($\times10^{-7}$, $M^{-1}cm^{-1}$)	$\sigma^{(1)}$[c] ($\times10^{-13}$, 3.1 eV)	$\sigma^{(2)}$[d] ($\times10^{6}$, GM, 1.55 eV)	QY (%)	τ_{XX} (ns, 1-photon)	$E_{b,xx}$ (meV)[b]	ASE minimum ($mJ\cdot cm^{-2}$ TPA)	G_{time} (ns, fluence)	$G_{bandwidth}$ (meV, $mJ\cdot cm^{-2}$, 10 ps delay)
4.5 nm	1.925	4.3	1.6	2.22	28	6.7	-48	1.5	5.88 (1.54)	277 (1.54)
6.0 nm	1.954	9.3	3.6	2.99	18	4.0	-64	1.7	3.43 (3.12)	193 (3.12 mJ/cm2)
8.2-nm-	1.774	9.2	3.5	9.58	13	11.9	-54	1.0	4.9 (3.12)	314 (2.19)

[a]Estimated from TEM sizing; total diameter

[b]Based upon second derivative minima of emission spectra at high intensity.

[c]From ICP of solutions with known absorption, using TEM-based sizing.

[d]Calculated from photoluminescence intensity versus Rhodamine 6G standard with two-photon excitation according to literature methods.

Given the large two-photon cross sections and previous demonstrations of low-threshold optical amplification, two-photon excitation was used to measure amplified spontaneous emission and lasing from the QS samples. Compared to one-photon excitation, frequency upconverting optical gain has advantages in homogeneity of excitation through the medium, weaker scattering of the pump excitation, and ease of cavity design. More generally, upconverted lasing is a useful alternative to non-linear optical conversions of coherent light.[21] To measure optical amplification, thin films of QSs were cast on to glass slides and amplified spontaneous emission (ASE) thresholds were measured by pumping the sample along a narrow stripe using a cylindrical lens. As shown in

Figure 3a, each QS sample exhibited ASE, characterized by the thresholded, non-linear emergence of a new, spectrally narrower emission feature. The first ASE feature of the QSs to appear with increasing pump fluence occurs on the blue side of the photoluminescence spectrum, indicating that it arises from a repulsive biexictonic emission. But, as shown in previous measurements on QS samples,[18] multiple ASE peaks occurred over a wide range of energy. In the cases of the 4.5 nm and 6.0 nm cores, ASE also occurs at an energy near the center of the photoluminescence feature, likely attributable to excitonic emission. For the 4.5 nm core and 8.2 nm cores, higher fluences result in ASE features even higher than the biexcitonic emission feature, due to filling of the band edge states. Corresponding transient absorption measurements of the samples (Figure S5) with 1.55 eV pumping confirm that the QSs can support a broad optical gain bandwidth as high as 300 meV and a gain lifetime of 3-6 nanoseconds, which is consistent with the long biexciton lifetimes. In addition to the spectral changes, ASE thresholds are analyzed in Figure 3b by measuring the emitted photon counts versus fluence, with thresholds apparent from the sharp increase of intensity at fluences ranging from 1.0-1.7 $mJ \cdot cm^{-2}$. The broad gain bandwidth, long gain lifetimes, and low two-photon ASE thresholds of these QS samples indicate potential for use as broadband gain media in a variety of cavity structures.

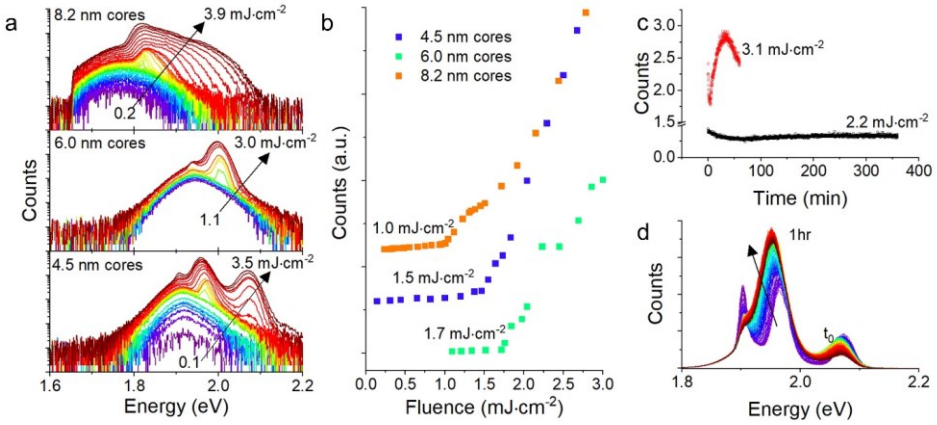

Figure 3. (a) Emission spectra as a function of fluence for CdS/CdSe/CdS QS thin film samples as a function of excitation fluence at 1.55 eV. A 750 nm short pass filter is used to block the pump light. (b) Emission counts of QS thin film samples versus laser fluence. (c) Integrated counts of 4.5 nm core quantum shells two values of fluence above the amplified spontaneous emission threshold. Data represents total integrated counts versus time. (d) Spectra of sample 4.5 nm core quantum shells displaying multimodal amplified spontaneous emission held at 3.1 mJ·cm^{-2} by stripe illumination for 1 hour. Violet spectra represent early time and red later times. Spectra were collected every 15 seconds for 1 hour.

Additionally, the stability of ASE in the samples was tested in air at room temperature. At modest fluences just above the ASE threshold for 4.5 nm core QSs, amplified emission lost 25 % of intensity over 50 minutes, but recovered over 6 hours (4.3×10^7 laser shots) to 90 % percent of initial signal (Figure 3c). At higher fluence (3.1 mJ·cm^{-2}), multimodal ASE was variable in both intensity and spectral response, also initially falling 25 %, then recovering to greater intensity than observed initially, which was accompanied by a redshift of the ASE bands and an increase in the biexcitonic band at the expense of excitonic and higher multiexciton bands (Figure 3d). Such variability of ASE is only possible due to the wide gain bandwidth of the QSs, but it may occur due to heating of the samples, which redshifts optical transitions,[51] or photocharging, which fills excitonic states.[52] In this area, both effects may be occurring, as the biexcitonic ASE feature increases in intensity over time (relative to the excitonic peak), and redshifts.

Commented [DBT5]: 10.1063/1.2001731

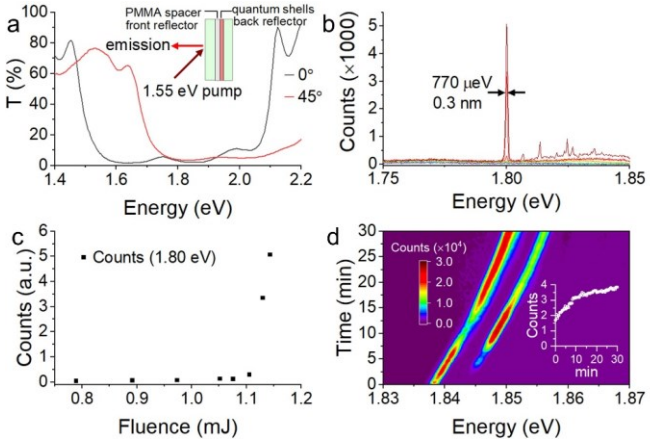

Figure 4. (a) Front window transmission of laser cavity for two-photon pumping of quantum shell sample. The pump beam is directed on to the sample at a 45° angle of incidence and the emission from the cavity is monitored normal to the surface, as shown inset. (b) Photoemission from laser cavity with 8.2 nm core quantum shells showing and (c) counts at 1.80 eV from the same cavity versus 1.55 eV pump fluence. Violet spectra represent lower fluence and red higher fluence. (d) Spectra as a function of time lapse for a different spot of the same cavity of 8.2 nm core quantum shells measured at a fixed fluence of 1.3 mJ·cm^{-2} 1.55 eV pump photons.

Finally, the QSs were used in an optically-pumped laser cavity. Two-photon pumped laser cavities have been demonstrated with several different nanomaterials, including CdSe quantum dots and platelets,[22,26,27,29,53–55] and perovskites.[56–59] The 8.2 nm core QS sample was deposited as a thin film via drop-casting in the simple laser cavity shown in Figure 4a. Two color-selective mirrors, with high normal-incidence reflectivity at 1.8 eV were sandwiched to form vertical-cavity surface-emitting laser. One mirror was coated with QSs and the other with a thin layer of PMMA to provide a spacer from the first mirror, a strategy employed earlier in similar Bragg grating lasers.[54] Because the mirror is semitransparent to the two-photon pump at 45°, the pump beam excites the sample at this angle, but the emission is monitored from the cavity at normal incidence. As shown in Figure 4b, a narrow emission line emerges at sufficiently high pump fluence. Initially a single laser line was observed at 1.80 eV with a band width of 770 μeV (0.3 nm), but at higher

fluence multiple modes are supported. The exact modes observed depend on the measured sample spot in the cavity; multimodal lasing was also previously observed under one-photon excitation in QSs.[60] The intensity of the optically-pumped laser shows clear thresholding behavior plotted in Figure 4c, with a fluence threshold of this laser slightly above 1.1 mJ·cm^{-2}. This threshold is slightly above the threshold for ASE of the same sample, but it should also be noted that the input fluence, measured before the sample, is partially diminished by the front mirror of the cavity and therefore the two thresholds are quite similar. A two-photon optically-pumped laser threshold of ~1 mJ·cm^{-2} is far below reported thresholds in quantum dots and (~6 mJ·cm^{-2}),[22,53] comparable to the lowest reported threshold for two-photon pumping in pure CdSe nanoplatelets (1.2 mJ·cm^{-2})[29] or dot-in-rod heterostructures (0.99 mJ·cm^{-2}),[26] but somewhat above the two-photon laser threshold for engineered CdSe core/shells (0.764 mJ·cm^{-2})[27] or perovskite nanocrystals (0.3 mJ·cm^{-2}).[58] Further improvement in the threshold both for ASE and lasing may be anticipated from QSs with improved emission quantum yields as well as film and cavity optimization.

As with ASE measurements above, the stability of the laser cavity emission was measured over time. In this case, initially a single mode is observed, but after 2 minutes, two laser modes are observed for the sample, both of which shift to the blue over time. In this case, the shift is approximately 10 meV in 30 minutes of measurement. Similar shifts in the mode of whispering gallery mode lasers from semiconductor nanocrystals were recently reported and attributed to changes in the index of the nanocrystal layer due to photocharging.[52] This explanation is also consistent with the small blueshift observed in the laser cavity in Figure 4d, in which photocharging, by slightly bleaching the band edge absorption transition, will reduce the refractive index and lead to the observed blueshift. In addition to the noted spectral shift, the intensity of the two modes varies over time and the absolute intensity of the laser cavity emission also increased

by a factor of two over 30 minutes. Again, this may be attributable to the same photocharging of the sample;[61–64] partial charging can lower the lasing threshold[61] and thereby produce a brighter laser over exposure time. These experiments suggests that higher stability of the emissive mode may be achieved with light soaking experiments[52] or by use of the QSs as flowed dyes.[29] As importantly, they also show that laser emission under two-photon excitation can be stable without a decrease in intensity over at least 3.6×10^5 laser shorts. The combination of large two-photon cross sections, long gain lifetimes, wide gain bandwidth, and low thresholds for amplified spontaneous emission indicates that QSs may also be strong candidates for nanoparticle-based dye lasers.

Conclusions.

CdS/CdSe/CdS QSs are shown to have large two-photon cross sections (up to 10^7 GM), which make QSs promising nanostructures for upconversion imaging applications. Two-photon cross-sections increase for the QSs with larger radius of curvature of the CdSe layer. These large two-photon cross-sections are combined with previously-identified advantages of QSs for multiexciton applications. Under two-photon excitation, QSs show large gain bandwidth (300 meV), long gain lifetime (>5 ns), and slow Auger recombination (>10 ns). Biexciton recombination times reaching greater than 10 ns drives many of these properties. The combination of large non-linear absorption cross-sections with long multiexciton lifetimes results in multimodal, low-threshold, amplified spontaneous emission and lasing under two-photon excitation with thresholds using 1.55 eV pumping as low as 1 $mJ\cdot cm^{-2}$.

ASSOCIATED CONTENT

Additional methods, data, and figures may be found in the supporting information file.

The following files are available free of charge.

Supporting Information (file type, i.e., PDF)

AUTHOR INFORMATION

Corresponding Author

*bdiroll@anl.gov

Author Contributions

The manuscript was written through contributions of all authors.

Notes

The authors declare no competing financial interest.

ACKNOWLEDGMENT

Work performed at the Center for Nanoscale Materials, a U.S. Department of Energy Office of Science User Facility, was supported by the U.S. DOE, Office of Basic Energy Sciences, under Contract No. DE-AC02-06CH11357. Work of BGSU team was supported by the award DE-SC0016872. MZ also acknowledges the support by NSF award #2208834.

REFERENCES

[1] N. Razgoniaeva, P. Moroz, M. Yang, D. S. Budkina, H. Eckard, M. Augspurger, D. Khon, A. N. Tarnovsky, M. Zamkov, *J. Am. Chem. Soc.* **2017**, *139*, 7815.
[2] D. Porotnikov, B. T. Diroll, D. Harankahage, L. Obloy, M. Yang, J. Cassidy, C. Ellison, E. Miller, S. Rogers, A. N. Tarnovsky, R. D. Schaller, M. Zamkov, *Nanoscale* **2020**, *12*, 17426.
[3] J. Cassidy, M. Zamkov, *J. Chem. Phys.* **2020**, *152*, DOI 10.1063/1.5126423.
[4] B. G. Jeong, Y. Park, J. H. Chang, I. Cho, J. K. Kim, K. Char, J. Cho, V. I. Klimov, P. Park, D. C. Lee, W. K. Bae, **2016**, DOI 10.1021/acsnano.6b03704.
[5] E. A. Dias, J. I. Saari, P. Tyagi, P. Kambhampati, *J. Phys. Chem. C* **2012**, *116*, 5407.

[6] N. Wang, S. Koh, B. G. Jeong, D. Lee, W. D. Kim, K. Park, M. K. Nam, K. Lee, Y. Kim, B. H. Lee, K. Lee, W. K. Bae, D. C. Lee, *Nanotechnology* **2017**, *28*, DOI 10.1088/1361-6528/aa6828.
[7] Z. Meng, B. Mahler, J. Houel, F. Kulzer, G. Ledoux, A. Vasil'ev, C. Dujardin, *Nanoscale* **2021**, 19578.
[8] J. Cassidy, D. Harankahage, D. Porotnikov, A. V. Malko, M. Zamkov, *ACS Energy Lett.* **2022**, *7*, 1202.
[9] G. Nagamine, B. G. Jeong, T. A. C. Ferreira, J. H. Chang, K. Park, D. C. Lee, W. K. Bae, L. A. Padilha, *ACS Photonics* **2020**, *7*, 2252.
[10] D. Battaglia, J. J. Li, Y. Wang, X. Peng, *Angew. Chem. Int. Ed. Engl.* **2003**, *42*, 5035.
[11] E. P. Pokatilov, V. A. Fonoberov, V. M. Fomin, J. T. Devreese, *Phys. Rev. B* **2001**, *64*, 245329.
[12] M. Braun, S. Link, C. Burda, M. El-Sayed, *Chem. Phys. Lett.* **2002**, *361*, 446.
[13] A. Hässelbarth, A. Eychmüller, R. Eichberger, M. Giersig, A. Mews, H. Weller, *J. Phys. Chem.* **1993**, *97*, 5333.
[14] D. Schooss, A. Mews, A. Eychmüller, H. Weller, *Phys. Rev. B* **1994**, *49*, 17072.
[15] J. Xu, M. Xiao, D. Battaglia, X. Peng, *Appl. Phys. Lett.* **2005**, *87*, 1.
[16] A. Eychmüller, A. Mews, H. Weller, *Chem. Phys. Lett.* **1993**, *208*, 59.
[17] D. Battaglia, B. Blackman, X. Peng, *J. Am. Chem. Soc.* **2005**, *127*, 10889.
[18] J. Cassidy, B. T. Diroll, N. Mondal, D. B. Berkinsky, K. Zhao, D. Harankahage, D. Porotnikov, R. Gately, D. Khon, A. Proppe, M. G. Bawendi, R. D. Schaller, A. V. Malko, M. Zamkov, *ACS Nano* **2022**, DOI 10.1021/acsnano.1c10404.
[19] F. Helmchen, W. Denk, *Nat. Methods* **2005**, *2*, 932.
[20] W. Denk, J. H. Strickler, W. W. Webb, *Science (80-.).* **1990**, *248*, 73.
[21] G. S. He, L. S. Tan, Q. Zheng, P. N. Prasad, *Chem. Rev.* **2008**, *108*, 1245.
[22] C. Zhang, F. Zhang, T. Zhu, A. Cheng, J. Xu, Q. Zhang, S. E. Mohney, R. H. Henderson, Y. A. Wang, *Opt. Lett.* **2008**, *33*, 2437.
[23] J. J. Jasieniak, I. Fortunati, S. Gardin, R. Signorini, R. Bozio, A. Martucci, P. Mulvaney, *Adv. Mater.* **2008**, *20*, 69.
[24] C. Bauer, B. Schnabel, E.-B. Kley, U. Scherf, H. Giessen, R. F. Mahrt, *Adv. Mater.* **2002**, *14*, 673.
[25] Y. Wang, V. D. Ta, Y. Gao, T. C. He, R. Chen, E. Mutlugun, H. V. Demir, H. D. Sun, *Adv. Mater.* **2014**, *26*, 2954.
[26] G. Xing, Y. Liao, X. Wu, S. Chakrabortty, X. Liu, E. K. L. Yeow, Y. Chan, T. C. Sum, *ACS Nano* **2012**, *6*, 10835.
[27] B. Guzelturk, Y. Kelestemur, K. Gungor, A. Yeltik, M. Z. Akgul, Y. Wang, R. Chen, C. Dang, H. Sun, H. V. Demir, *Adv. Mater.* **2015**, *27*, 2741.
[28] M. Olutas, B. Guzelturk, Y. Kelestemur, A. Yeltik, S. Delikanli, H. V. Demir, *ACS Nano* **2015**, *9*, 5041.
[29] M. Li, M. Zhi, H. Zhu, W.-Y. Y. Wu, Q.-H. H. Xu, M. H. Jhon, Y. Chan, *Nat. Commun.* **2015**, *6*, 1.
[30] G. S. He, P. P. Markowicz, T.-C. Lin, P. N. Prasad, *Nature* **2002**, *415*, 767.
[31] Q. Zheng, H. Zhu, S. C. Chen, C. Tang, E. Ma, X. Chen, *Nat. Photonics* **2013**, *7*, 234.
[32] C. Zhang, C. L. Zou, Y. Yan, R. Hao, F. W. Sun, Z. F. Han, Y. S. Zhao, J. Yao, *J. Am. Chem. Soc.* **2011**, *133*, 7276.
[33] C. F. Zhang, Z. W. Dong, G. J. You, S. X. Qian, H. Deng, *Opt. Lett.* **2006**, *31*, 3345.

[34] B. T. Diroll, N. Gogotsi, C. B. Murray, *Chem. Mater.* **2016**, *28*, 3345.
[35] A. Sitt, F. Della Sala, G. Menagen, U. Banin, *Nano Lett.* **2009**, *9*, 3470.
[36] A. F. Cihan, Y. Kelestemur, B. Guzelturk, H. V. Demir, **2013**, *1*, 5.
[37] V. I. Klimov, *Science* **2000**, *287*, 1011.
[38] I. Robel, R. Gresback, U. Kortshagen, R. D. Schaller, V. I. Klimov, *Phys. Rev. Lett.* **2009**, *102*, 177404.
[39] C. Melnychuk, P. Guyot-Sionnest, *Chem. Rev.* **2021**, *121*, 2325.
[40] Y. S. Park, W. K. Bae, L. A. Padilha, J. M. Pietryga, V. I. Klimov, *Nano Lett.* **2014**, *14*, 396.
[41] Y. He, S. Hu, T. Han, X. Chen, Y. Yu, T. Li, W. Zhu, G. Ouyang, *ACS Omega* **2019**, *4*, 9198.
[42] C. She, I. Fedin, D. S. Dolzhnikov, P. D. Dahlberg, G. S. Engel, R. D. Schaller, D. V. Talapin, *ACS Nano* **2015**, *9*, 9475.
[43] V. I. Klimov, *Annu. Rev. Condens. Matter Phys.* **2014**, *5*, 285.
[44] G. E. Cragg, A. L. Efros, *Nano Lett.* **2010**, *10*, 313.
[45] R. Scott, A. W. Achtstein, A. Prudnikau, A. Antanovich, S. Christodoulou, I. Moreels, M. Artemyev, U. Woggon, *Nano Lett.* **2015**, *15*, 4985.
[46] A. W. Achtstein, A. Ballester, J. L. Movilla, J. Hennig, J. I. Climente, A. Prudnikau, A. Antanovich, R. Scott, M. V. Artemyev, J. Planelles, U. Woggon, *J. Phys. Chem. C* **2015**, *119*, 1260.
[47] M. A. Albota, C. Xu, W. W. Webb, *Appl. Opt.* **1998**, *37*, 7352.
[48] J. P. Hermann, J. Ducuing, *Opt. Commun.* **1972**, *6*, 101.
[49] C. Xu, W. W. Webb, *J. Opt. Soc. Am. B* **1996**, *13*, 481.
[50] M. Allione, A. Ballester, H. Li, A. Comin, J. L. Movilla, J. I. Climente, L. Manna, I. Moreels, *ACS Nano* **2013**, *7*, 2443.
[51] B. T. Diroll, A. Brumberg, R. D. Schaller, *Sci. Rep.* **2022**, *12*, 1.
[52] S. J. Neuhaus, E. Marino, C. B. Murray, C. R. Kagan, *Nano Lett.* **2023**, *23*, 645.
[53] B. Guzelturk, Y. Kelestemur, M. Z. Akgul, V. K. Sharma, H. V. Demir, *J. Phys. Chem. Lett.* **2014**, *5*, 2214.
[54] B. Guzelturk, Y. Kelestemur, M. Olutas, S. Delikanli, H. V. Demir, *ACS Nano* **2014**, *8*, 6599.
[55] D. Dede, N. Taghipour, U. Quliyeva, M. Sak, Y. Kelestemur, K. Gungor, H. V. Demir, *Chem. Mater.* **2019**, *31*, 1818.
[56] L. Xu, Y. Meng, C. Xu, P. Chen, *RSC Adv.* **2018**, *8*, 36910.
[57] Y. Xu, Q. Chen, C. Zhang, R. Wang, H. Wu, X. Zhang, G. Xing, W. W. Yu, X. Wang, Y. Zhang, M. Xiao, *J. Am. Chem. Soc.* **2016**, *138*, 3761.
[58] Z. Liu, Z. Hu, Z. Zhang, J. Du, J. Yang, X. Tang, W. Liu, Y. Leng, *ACS Photonics* **2019**, *6*, 3150.
[59] J. Ban, Y. Yu, P. Yue, L. Lian, C. Xu, L. Guo, S.-D. Liu, *J. Phys. Chem. C* **2022**, *126*, 8400.
[60] J. Xu, M. Xiao, *Appl. Phys. Lett.* **2005**, *87*, 1.
[61] C. Wang, B. L. Wehrenberg, C. Y. Woo, P. Guyot-Sionnest, *J. Phys. Chem. B* **2004**, *108*, 9027.
[62] K. Wu, Y. Park, J. Lim, V. I. Klimov, *Nat. Nanotechnol.* **2017**, *12*, 1140.
[63] Y. S. Park, J. Roh, B. T. Diroll, R. D. Schaller, V. I. Klimov, *Nat. Rev. Mater.* **2021**, *6*, 382.
[64] O. V Kozlov, Y. Park, J. Roh, I. Fedin, T. Nakotte, V. I. Klimov, *Science (80-.).* **2019**, *365*, 672.

Supporting Information

Low-Threshold Multiphoton Gain and Lasing of CdS/CdSe/CdS Quantum Shells

Benjamin T. Diroll,[1] *James P. Cassidy, Dulanjan Harankahage, Mikhail Zamkov, ...* [1]*Center for Nanoscale Materials, Argonne National Laboratory. 9700 S. Cass Avenue, Lemont, Illinois 60439, United States*

Experimental

Materials.

Synthesis.

Structural Characterization. X-ray diffraction was performed using a Bruker D2-phaser with samples drop-cast on to a miscut silicon sample holder with copper k-alpha X-rays. Transmission electron microscopy (TEM) was performed using a JEOL 2100F. The core, total sample size, and thickness of the CdSe layer was determined by TEM. The thickness of the CdSe layers of the samples, which was evaluated using electron microscopy, was 1.9 nm, 1.4 nm, and 1.7 nm for the 4.5 nm, 6.0 nm, and 8.5 nm CdS cores.

Steady-state Spectroscopy. Absorption spectra of the samples were recorded using a Perkin-Elmer Lambda 950. Photoluminescence was collected using a lamp excitation on a Horbia Jobin-

Commented [DBT6]: details

Commented [DBT7]: details

Commented [DBT8]: And another from BGSU work.

Yvon Fluorolog spectrometer. Power-dependent photoluminescence spectra were collected under 1.55 eV (800 nm) excitation and 3.10 eV (400 nm, by frequency doubling of the amplified Ti: sapphire fundamental). The geometry of the measurement was the same for both samples (front face) in cuvettes, with power measured in front of the sample. Photoluminescence was collected into a fiber and spectrally dispersed on to a CCD. The acquisition conditions were kept fixed in terms of wavelength, integration time, and acquisitions, but the repetition rate of the laser was adjusted (from 2 kHz to 20 Hz) to ensure that the CCD was not saturated. For stripe excitation measurements the 1.55 eV fundamental of the Ti: sapphire laser was pulsed at 200 Hz and focused on to thin films coated of QSs coated on to glass, with emitted light collected in the sample plane (normal to excitation). For lasing cavity measurements, a laser cavity was made using two color-filtering mirrors (Thorlabs): one was coated with polymethylmethacrylate to provide a small spacer and the other with QS samples. The pair of mirrors was sandwiched together and positioned at 45° with respect to an 1.55 eV pump beam which was focused on to the active layer of the cavity. Emitted light was collected normal to the surface. In both stripe and cavity measurements, power was measured just before the sample.

Extinction Coefficient Measurements. Extinction coefficients are estimated in this work by taking the absorption spectra of well-washed samples (to remove any additional ligand or unbound cadmium carboxylate), digesting the sample with aqua regia (high purity nitric and hydrochloric acid), and measuring the concentration of cadmium in the solution at defined dilutions using ICP-OES (Agilent). Measurements were performed in triplicate, then the cadmium concentration was used to estimate the concentration of QS based upon the size observed from TEM.

Time-resolved photoluminescence. The configuration of time-resolved photoluminescence was the same as power-dependent photoluminescence measurements, but instead of focusing the output photoluminescence into a fiber, it was directed into a streak camera (Hamamatsu). At higher fluence excitation, the photoluminescence was attenuated using a broadband neutral density filter wheel placed in front of the streak camera, to ensure single photon sensitivity.

Transient Absorption. Transient absorption was performed by splitting the fundamental output of a 35 fs Ti: sapphire laser into pump and probe branches. The pump branch was chopped to 1 kHz; the probe branch was focused through a 2 mm sapphire plate to generate a supercontinuum white light. The pump and probe are spatially overlapped at the sample position and pump-probe delay is adjusted using a delay stage. To ascertain the gain spectrum, the change in absorption measured in transient absorption is added to the static absorption.

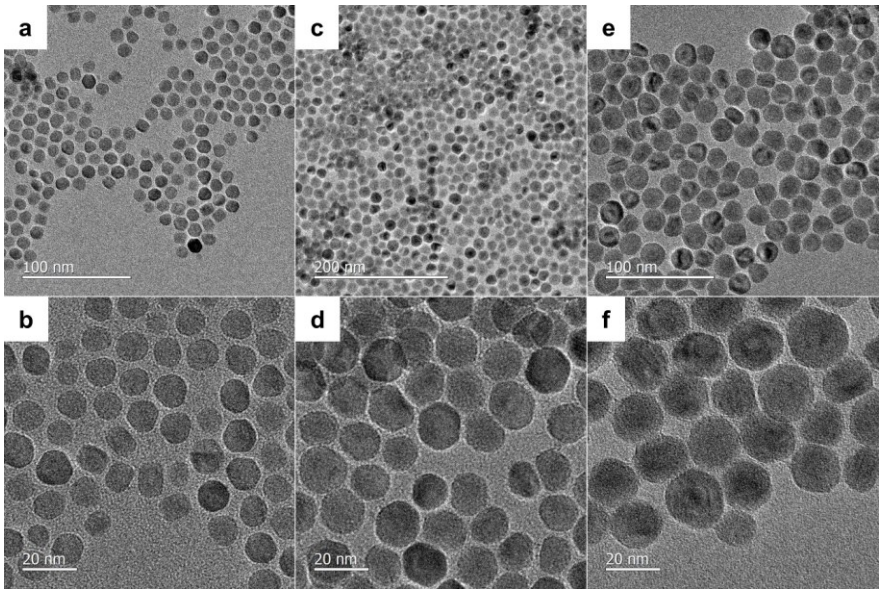

Figure S1. Transmission electron micrographs of (a, b) 6.0 nm core QSs, (c, d) 4.5 nm core QSs, and (e, f) 8.2 nm core QSs.

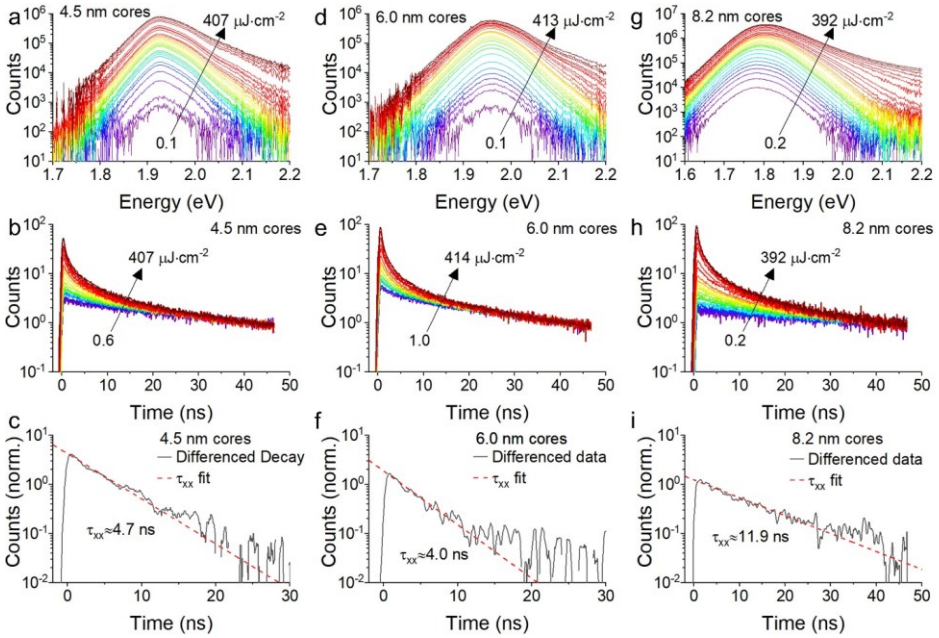

Figure S2. (a) Fluence-dependent photoluminescence spectra of 4.5 nm core QSs with 3.10 eV pump. (b) Time-resolved photoluminescence of 4.5 nm QSs with 3.10 eV pump. (c) Differenced data from (b) and monoexponential decay fit to extract biexciton lifetime. (d-f) Analogous data from 6.0 nm core QSs and (g-i) 8.2 nm core QSs.

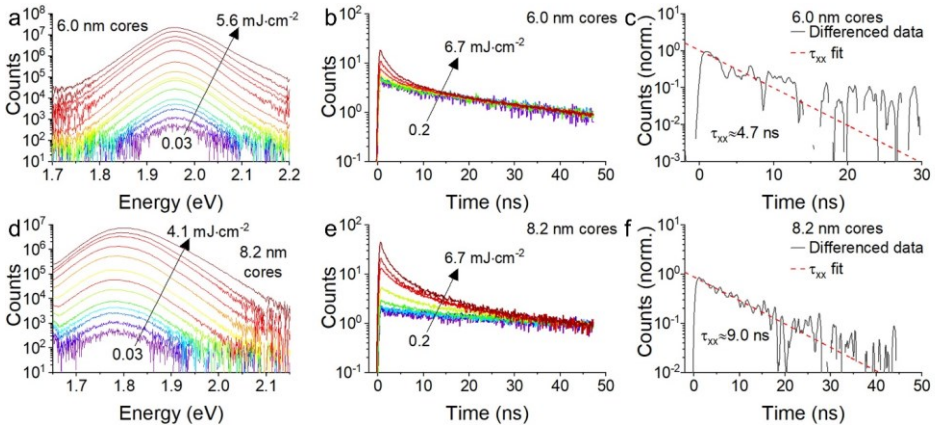

Figure S3. (a) Photoluminescence intensity with increasing pump 1.55 eV pump fluence for sample 6.0 nm core QSs. (b) Time-resolved photoluminescence of 6.0 nm core quantum shells normalized at ~50 ns delay for a series of increasing pump fluence. (c) Differenced data from (b) and monoexponential decay fit to extract biexciton lifetime. (d-f) analogous data from sample 8.2 nm core QSs.

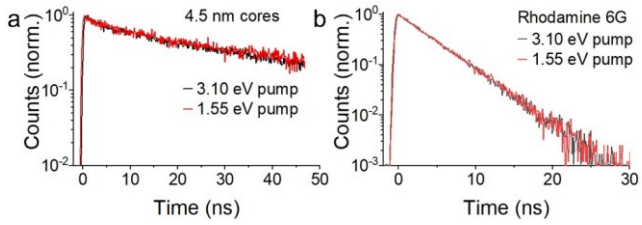

Figure S4. (a) Comparison of photoluminescence lifetime of 4.5 nm core quantum shell and (b) Rhodamine 6G dissolved in ethanol with 3.10 eV and 1.55 eV pump excitation.

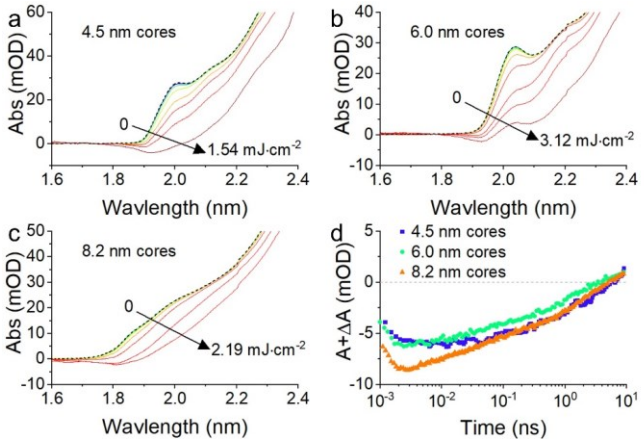

Figure S5. Gain spectra of (a) 4.5 nm core quantum shells, (b) 6.0 nm core quantum shells, and (c) 8.2 nm core quantum shells with 1.55 eV pumping. Dashed black lines show the absorption spectrum the sample without pump excitation. (d) Kinetics of gain at the energy of maximum gain for each sample at fluences of 1.54, 3.12, and 2.19 mJ·cm^{-2} respectively.